Available online at www.sciencedirect.com
SCIENCE DIRECT®
Journal of Power Sources 117 (2003) 212–222
JOURNAL OF POWER SOURCES
www.elsevier.com/locate/jpowsour

Experimental study of the thermal behavior of a water cooled Ni–Cd battery

Jean-Michel Mottard[1], Cécile Hannay[1], Eric L. Winandy[*]

Laboratory of Thermodynamics, University of Liège, Campus du Sart Tilman-Bât. B49, B-4000 Liège, Belgium

Received 2 June 2002; received in revised form 19 December 2002; accepted 22 December 2002

Abstract

In this paper, the Ni–Cd battery principle and exothermal processes are first recalled. It is pointed out that heat generation can be decomposed into irreversible losses (entropic effect), battery electric resistance and polarization effect. It is shown how these effects can be analyzed from overall battery heat balance. The calorimetric test bench is described. Battery cycles are composed of charge, overcharge, rest and discharge. Typically, the total heat losses range around 25% with an increase up to 33% at 200 A. Only during overcharge, gas losses are shown to be a high contribution. The paper shows that the calorimetric study permits not only further insight into local temperatures and heat losses, but also to deduce such parameters as entropy generation and, above all, total resistance (Joule effect and polarization). In this case, resistance was estimated to increase from 2 to 6 mΩ with depth of discharge from 0 to 100%.

Keywords: Ni–Cd battery; Thermodynamics; Thermal behavior; Heat balance; Entropy generation; Electric resistance; Battery cycle; Experimental analysis

1. Introduction

Battery thermal behavior is an important concern since it influences its longevity. Battery processes are indeed largely exothermic and the heat produced has to be well controlled in order not to destroy the battery due to temperature rise.

Calorimetric studies are important to analyze the different modes of heat generation and how they can be influenced. For example, it helps to understand the gas production process during overcharge as well as to show hot spots inside the battery block and support the cooling network designer [1–4].

In this paper, it is shown that an accurate heat balance can be used to do more than a global analysis. It is shown how it is possible to deduce battery intrinsic parameters such as entropy generation and electrical resistance at different depths of discharge (DOD).

The example taken here is the Ni–Cd battery. Ni–Cd and nickel-based rechargeable batteries are still expanding and still under research 30 years after their first commercialization [5,6].

2. Operating principle of the Ni–Cd battery

The Ni–Cd battery tested here comprises a positive electrode of NiOOH and a negative electrode of Cd. The governing reactions occurring during the Ni–Cd battery charge and discharge processes are [7]:

Positive electrode:

$$2\mathrm{NiOOH} + 2\mathrm{H_2O} + 2\mathrm{e^-} \underset{\text{charge}}{\overset{\text{discharge}}{\rightleftarrows}} 2\mathrm{Ni(OH)_2} + 2\mathrm{OH^-} \quad (1)$$

Negative electrode:

$$\mathrm{Cd} + 2\mathrm{OH^-} \underset{\text{charge}}{\overset{\text{discharge}}{\rightleftarrows}} \mathrm{Cd(OH)_2} + 2\mathrm{e^-} \quad (2)$$

Global reaction:

$$\mathrm{Cd} + 2\mathrm{NiOOH} + 2\mathrm{H_2O} \underset{\text{charge}}{\overset{\text{discharge}}{\rightleftarrows}} \mathrm{Cd(OH)_2} + 2\mathrm{Ni(OH)_2} \quad (3)$$

As the positive electrode is charged less easily than the negative one [8], it results in a dioxygen release at the positive electrode, when the status of full charge is approached:

$$4\mathrm{OH^-} \rightarrow 2\mathrm{H_2O} + \mathrm{O_2} + 4\mathrm{e^-} \quad (4)$$

Thus, at the beginning of gas release, there is almost only dioxygen.

[*] Corresponding author. Tel.: +32-4-3664802; fax: +32-4-3664812.
E-mail addresses: jmmottard@yahoo.fr (J.-M. Mottard), eric.winandy@planetmail.com (E.L. Winandy).
[1] Tel.: +32-4-3664800; fax: +32-4-3664812.

0378-7753/03/$ – see front matter © 2003 Elsevier Science B.V. All rights reserved.
doi:10.1016/S0378-7753(03)00004-1

Nomenclature

A	area (m^2)
c	specific heat ($J\ kg^{-1}\ K^{-1}$)
C	heat capacity ($J\ K^{-1}$)
CAP	electric capacity (C)
DOD	depth of discharge
e	depth (m)
E	zero load battery voltage (V)
F	number of Faraday (96,487 $C\ mol^{-1}$)
G	free energy (J)
h	heat transfer coefficient ($W\ m^{-2}\ K$)
H	enthalpy (J)
HHV	higher heating value ($J\ kg^{-1}$)
I	current intensity (A)
k	thermal conductivity ($W\ m^{-1}\ K^{-1}$)
$\dot{M}$	mass flow rate ($kg\ s^{-1}$)
Q	heat (J)
$\dot{Q}$	heat flow (W)
R	resistance (Ω)
S	entropy ($J\ K^{-1)}$
T	temperature (K)
U	internal energy (J)
$\dot{W}$	power (W)
z	number of mole of electrons (mol)

Greek letters

α	overcharge ratio
ε	cooling pump efficiency
τ	time (s)

Subscripts

+	positive side
−	negative side
a	position "a"
amb	battery external environment (ambient)
b	position "b"
bat	battery
br	cooling loop
c	charge, central (sensor position inside the battery stack)
d	discharge
eq	equilibrium
ex	exhaust
f	final
hex	heat exchanger
H_2	dihydrogen
i	initial
j	number of face j
loss	losses
p	thermocouple position on the wall inside the battery stack
P	pressure
r	reaction
ref	reference
res	resistance
s	entropic or surface (sensor position)
su	supply
th	thermoneutral
w	water

On the other hand, the negative electrode accepts charge up to nearly 100% of nominal capacity. After that, it starts producing dihydrogen:

$$4H_2O + 4e^- \rightarrow 2H_2 + 4OH^- \quad (5)$$

As we can see, dioxygen and dihydrogen are not released in equal amount.

During the overcharge phase, a fraction of the current injected in the battery is used to carry out water electrolysis:

$$2H_2O \rightarrow 2H_2 + O_2 \quad (6)$$

Thus after every charge process, the battery loses a small amount of water. This is why it is necessary to refill the battery with distilled water after every test campaign. The battery is then not open proof.

3. Analysis of the battery's exothermic process

3.1. Thermoneutral voltage

During a chemical reaction, the variation of free energy is equal to the theoretical maximum work, at constant temperature and pressure. In other words, it is equal to the work done reversibly. For an electrochemical reaction, the electric work is given by:

$$\Delta G = -zFE_{eq} \quad (7)$$

We adopt the convention that any work done by the battery is considered negative. For a chemical reaction, at constant temperature, the variation of free energy can also be written:

$$\Delta G = \Delta H - T\Delta S \quad (8)$$

We define the thermoneutral electromotive force E_{th} as the voltage for which the variation of entropy during reaction (exchanged and created) is equal to 0. So we have:

$$E_{th} = -\frac{\Delta H}{zF} \quad (9)$$

Recording that the entropy variation for a system in thermodynamic equilibrium can be written:

$$\Delta S = \Delta\left(\frac{\partial G}{\partial T}\right)_P \quad (10)$$

applied to Eq. (7) and replacing in Eq. (8), we get the following equation:

$$E_{th} = E_{eq} - T\frac{\partial E_{eq}}{\partial T} \quad (11)$$

The thermoneutral voltage E_{th} is the voltage of the battery at a temperature of 0 K, when delivering no current.

3.2. Battery losses

The heat losses produced in the battery come from different sources:

- entropic effect,
- battery's electrical resistance,
- polarization effect, which comes from the fact that some energy is required for diffusion of ions in the electrolyte,
- self-discharge effects.

In the following equations, we will disregard self-discharge effects and also group electrical resistance and polarization resistance in one resistance called "internal resistance".

So we can write:

$$\dot{Q}_{loss} = \dot{Q}_{res} + \dot{Q}_s \tag{12}$$

where $\dot{Q}_{res}$ are the heat losses due to resistive dissipation and $\dot{Q}_s$ due to entropy increase. In discharge (when $E_{eq} > E$), these different terms can be written:

$$\dot{Q}_{res} = -zF(E_{eq} - E) \tag{13}$$

$$\dot{Q}_s = T\Delta S = zFT\frac{\partial E_{eq}}{\partial T} \tag{14}$$

We obtain:

$$\dot{Q}_{loss} = -zF(E_{th} - E) \tag{15}$$

It can be seen that the thermoneutral voltage is given when there is no heat dissipation. The total heating power is obtained from the derivative of total heat generated in the battery with respect to time:

$$\dot{Q}_{loss} = \frac{\Delta Q_{loss}}{\Delta\tau} = I(E_{th} - E) \tag{16}$$

with I being positive for charging process and negative for discharging process.

3.3. Internal resistance

Introducing internal resistance R, the heating power due to internal resistance can be written:

$$\dot{Q}_{res} = -RI^2 \tag{17}$$

As total heating power is the addition of internal resistance heating power and entropic effect heating power, we have:

$$\dot{Q}_{loss} = I(E_{th} - E) = -RI^2 - IT\frac{\partial E_{eq}}{\partial T} \tag{18}$$

Dividing each member of this equation by I leads to:

$$E_{th} - E = -RI - T\frac{\partial E_{eq}}{\partial T} \tag{19}$$

Eq. (19) will be used to determine internal resistance R and entropy variation during discharge on a basis of experimental calorimetric tests.

4. Description of test apparatus

The battery tested in our calorimetric test bench has a nominal capacity of 100 Ah and a nominal voltage of 6 V. It is composed of five cells connected in series. Due to its inherent losses, the battery has to be cooled when working on charge or discharge. For that reason, it is equipped with a cooling system supplied with water. The test bench presented here below is able to measure not only voltage and current provided to or going out of the battery but also battery heat losses as well as gases produced during water electrolysis.

In order to ensure good accuracy of tests results, special care has to be taken of the battery cooling system.

4.1. Battery cooling system

The cooling system of the battery is presented in Fig. 1. The battery external surface is isolated as presented in Fig. 2. All the sides are covered by a layer of 0.04 m of expanded polystyrene, except the upper face filled with a layer of 0.08 m of small balls of polystyrene. The isolated battery is put in a wood box with 0.018 m thick wall. The battery heat

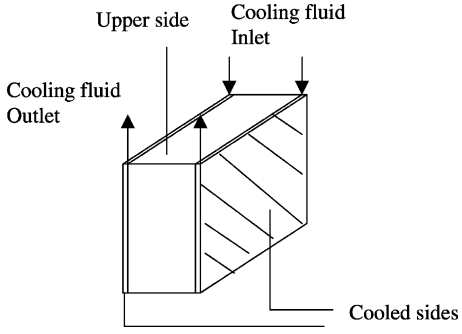

Fig. 1. Battery cooling.

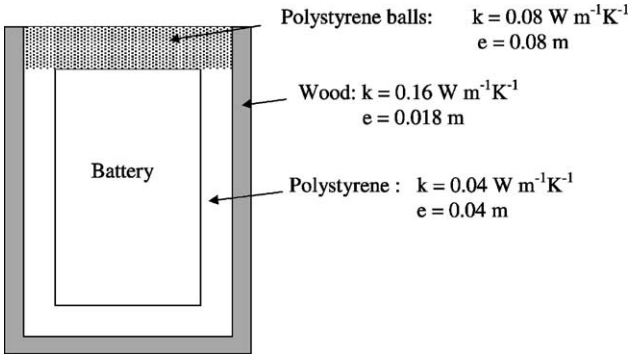

Fig. 2. Thermal isolation of the battery.

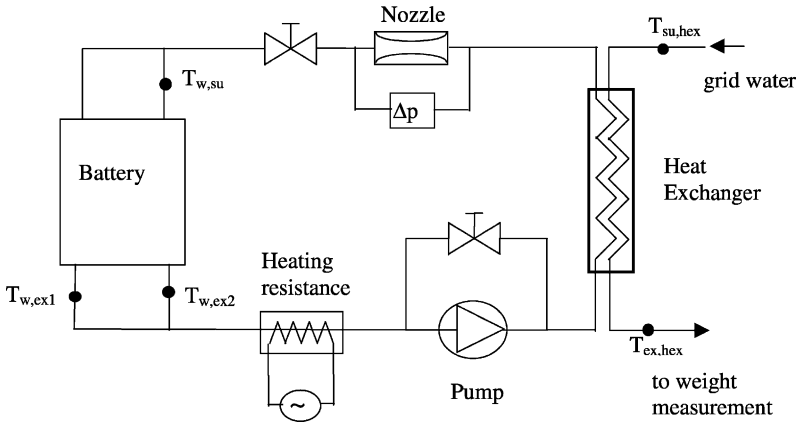

Fig. 3. Cooling network.

exchange coefficient to the ambient was determined experimentally to $h_{bat} = 0.808\ W\ m^{-2}\ K^{-1}$.

The external cooling loop is shown in Fig. 3 and it consists of:

- an aquarium type pump of low power,
- a nozzle to measure the mass flow rate,
- a by-pass in order to adjust the water mass flow rate,
- an electric heating resistance of 80 W,
- two cooling coils to regulate cooling fluid temperature in the loop. The cooling fluid mass flow rate is measured by weight accumulation. The cooling fluid is water.

The battery was equipped with 10 type *K* thermocouples inside (Fig. 4): two in each cell (*j*), one in the center of the stack ($T_{c,j}$) and the other one stuck on the wall ($T_{p,j}$). In order to measure the battery superficial temperatures, eight type *T* thermocouples were installed ($T_{s,j}$): three were installed on the upper face and one on each other face (Fig. 4). In order to ensure a reliable measurement of the average temperature on the wall, each thermocouple was welded on a copper plate (0.1 m × 0.1 m × 0.0002 m). The electric connections + and − to the battery were carried out thanks to copper rods (transversal section: 0.015 m × 0.003 m). In order to minimize heat losses through these rods, these were placed under a layer of small balls of polystyrene on a length of 0.35 m. Four thermocouples were placed on these electric connections (Fig. 4): directly on the mono-block connection (T_{+a} and T_{-a}) and at 0.15 m of the connection (T_{+b} and T_{-b}).

4.2. Charging and discharging system

4.2.1. Charging system

The battery is charged by a car alternator rectifier driven at constant revolution speed by an asynchronous motor. Voltage is adjusted by varying the alternator excitation current.

4.2.2. Discharging system

For discharge currents higher than 50 A, the battery is feeding a liquid rheostat where electrolysis of water is carried out. In order to maintain the discharge current as constant as possible, the electrolyte level in the liquid rheostat needs to be adjusted manually.

Battery voltage is directly measured by the data acquisition system. Current intensity is measured as voltage drop at a shunt of $2 \times 10^{-4}\ \Omega$. These shunts were calibrated to ensure an accuracy of 0.5%.

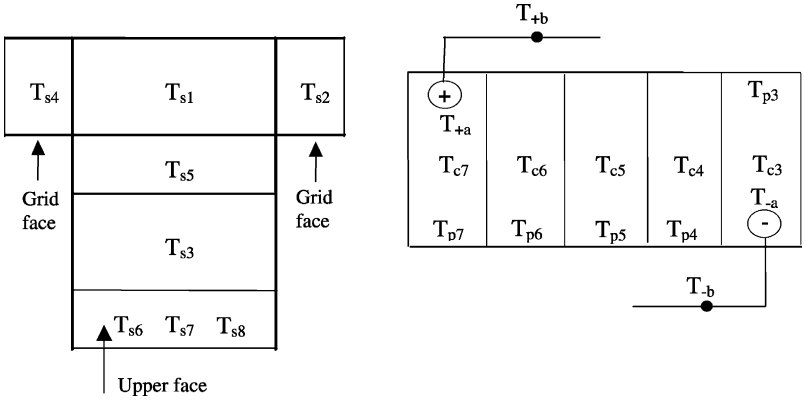

Fig. 4. Position of the thermocouples on a split view of the battery.

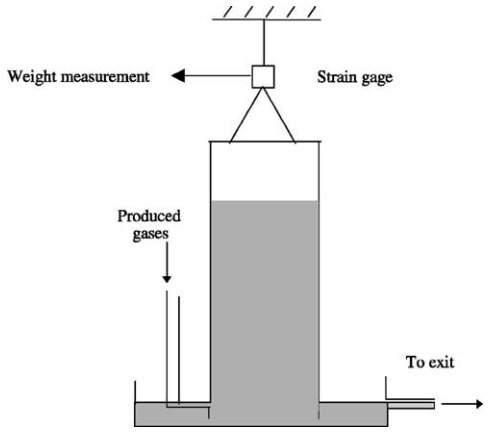

Fig. 5. Measurement of the quantity of gas produced by the battery.

4.3. Measurement of the quantity of gas produced by the battery

During overcharging, oxygen and hydrogen are produced by electrolysis of water. The apparatus presented in Fig. 5 was used to measure the volume of produced gases. As the gases are produced, they accumulate in the tank and displace the water that was contained there. The force sensor measures the decrease of the mass of the tank during the discharge phase. It is then possible to deduce the quantity of water that went out of the battery.

5. Thermal balances

The general battery thermal balance is given by Eq. (20) (illustrated in Fig. 6). Note the different terms can be positive, negative or nulls following the phase (see Table 4) and this, in agreement with the convention adopted in Section 3.1:

$$\frac{dU_{bat}}{d\tau} = EI + \dot{M}_{w,bat} c_w (T_{w,su} - T_{w,ex}) + \sum_j A_{bat-j} h_{bat} (T_{amb} - T_{s,j}) - \frac{d\dot{M}_{H_2}}{d\tau} HHV_{H_2} \quad (20)$$

The battery internal energy increase can be split into two different terms: one term for the accumulation of thermal energy and the other in chemical mode, corresponding to the oxydo-reduction reaction occurring in battery.

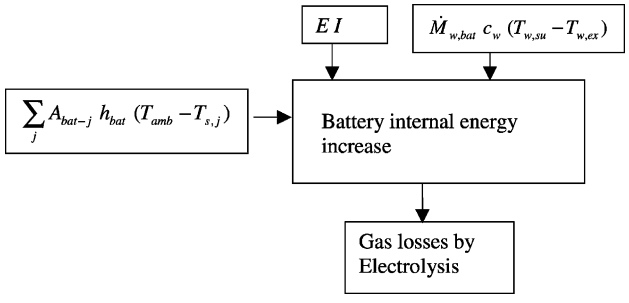

Fig. 6. General battery thermal balance. Note the different term scan be positive, negative or nulls following the phase (see Table 4).

We can write then:

$$\frac{dU_{bat}}{d\tau} = \left[\frac{dU_{bat}}{d\tau}\right]_{thermal} + \left[\frac{dU_{bat}}{d\tau}\right]_{chemical} = \sum_j C_{bat-j} \frac{dT_{bat-j}}{d\tau} + E_{th} I \quad (21)$$

And if we introduce the power losses given by Eq. (16), we get:

$$\sum_j C_{bat-j} \frac{dT_{bat-j}}{d\tau} = \dot{Q}_{loss} + \dot{M}_{w,bat} c_w (T_{w,su} - T_{w,ex}) + \sum_j A_{bat-j} h_{bat} (T_{amb} - T_{s,j}) - \frac{d\dot{M}_{H_2}}{d\tau} HHV_{H_2} \quad (22)$$

During the different phases, the thermal balance becomes:

Rest: The current intensity through the battery is zero, so the heating power is also reduced to zero and there is no gas production.

Charge: Current intensity is taken with a positive sign.

Discharge: Current intensity is taken with a negative sign, and there is no gas production.

5.1. Cooling system thermal balance

Because of the small temperature difference between $T_{w,ex}$ and $T_{w,su}$ (about 0.1 K), the contribution of the cooling system to the battery heat balance was not measured directly. It was determined by thermal balance on the cooling loop:

$$C_{br} \frac{dT_{br}}{d\tau} = \varepsilon \dot{W}_{pump} + \dot{M}_{w,hex} c_w (T_{su,hex} - T_{ex,hex}) + (Ah)_{br} (T_{amb} - T_{br}) - \dot{M}_{w,bat} c_w (T_{w,su} - T_{w,ex}) \quad (23)$$

Note that the useful pump power is neglected: indeed it represents only 7% of the total pump power which is 6 W! In other words, the water mass flow rate through the heat exchanger $\dot{M}_{w,hex}$ is imposed much lower than $\dot{M}_{w,bat}$ through the battery to increase the temperature difference $(T_{su,hex} - T_{ex,hex})$ to a measurable magnitude. Knowing the heat flow through the heat exchanger, it is easy to deduce the battery heating or cooling through the heat balance Eq. (23).

6. Description of the tests

Before each cycle, the battery was set in thermal equilibrium with the cooling loop and its climatized environment. The whole charge and discharge cycle includes six phases (see Fig. 7).

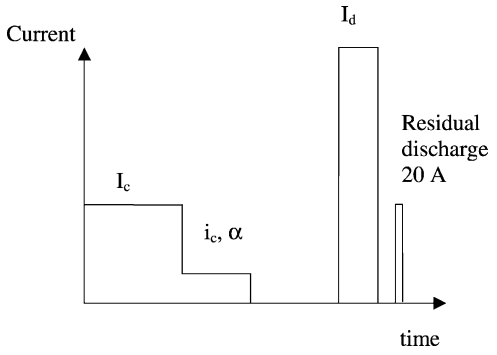

Fig. 7. Charging and discharging cycle.

Table 1
Cutting voltage vs. current intensity

Regime	Current intensity (A)	Cutting voltage (V)
CAP/5	20	5.0
CAP	100	4.5
2CAP	200	4.0

Charge: During this phase, the battery is charged with a current intensity I_c up to the commutation voltage. The battery reached then capacity CAP_c (in coulombs).

Overcharge: During this phase, the battery is charged at constant current i_c, up to the capacity αCAP_c (in coulombs), where α is the overcharge rate.

Rest: The battery is left alone for a sufficient time in order to reach thermal equilibrium with the cooling loop and with its environment. The battery temperature is then identical to that before charge.

Discharge: The battery is discharged at constant current I_d. Discharge is stopped when a certain voltage (cut-off voltage) has been reached. This voltage depends on the discharging regime as indicated in Table 1.

Residual discharge: The objective of this phase is to impose the same chemical state at the end of all cycles.

Rest: During this phase, the battery is resting until it reaches thermal equilibrium with its environment. This way, temperatures at the beginning and at the end of tests are very close and this results in a very low capacitive term of the heat balance. The test program is given in Table 2.

Table 2
Test program

No.	I_c (A)	i_c (A)	Overcharge	I_d (A)
1	20	5	0.15	20
2	20	5	0.15	30
3	20	5	0.15	50
4	20	5	0.15	100
5	20	5	0.15	150
6	20	5	0.15	200

7. Results

7.1. Thermal balances by phase

The thermal balances written here before have to be integrated if it is aimed at analyzing a particular phase. Also it is possible to evaluate the global residue for the whole cycle by:

$$\text{residue} = \int_{\text{charge}} EI_c\,d\tau + \int_{\text{overcharge}} Ei_c\,d\tau + \int_{\text{discharge}} EI_d\,d\tau + \sum \text{losses} - \sum_j C_{\text{bat}-j}\Delta T_{\text{bat}-j}\Big|_{\tau_i}^{\tau_f} \quad (24)$$

where we noted:

$$\sum \text{losses} = \sum_j A_{\text{bat}-j}h_{\text{bat}}\int_{\tau_i}^{\tau_f}(T_{\text{amb}} - T_{s,j})\,d\tau + \int_{\tau_i}^{\tau_f}\dot{M}_{w,\text{bat}}c_w(T_{w,\text{su}} - T_{w,\text{ex}})\,d\tau - \dot{M}_{H_2}\text{HHV}_{H_2} \quad (25)$$

In order to illustrate these results in a relative way, the thermal balances were divided by the total electric energy given to the battery:

$$\int_{\text{charge}} EI_c\,d\tau + \int_{\text{overcharge}} Ei_c\,d\tau$$

An example of such balance is given in Tables 3 and 4 for test no. 4, $I_c = 20$ A, $\alpha = 0.15$, $I_d = 100$ A. Table 3 presents the global balance showing that the overall losses reach almost 30%. Table 4 presents the thermal balance phase by phase: battery ambient losses are negligible for all phases, thermal losses to the cooling system are the most important during overcharge, rest phases and discharge. In the charging phase joule and polarization heat generation is compensated by heat absorption of the endothermic reaction. We can also see that the cooling system is heating the battery during the charging period. Losses due to water electrolysis are the most important in the overcharging phase (about 16 W) and the dynamic contribution is linked to the temperature gradients during overcharging, resting

Table 3
Global thermal balance for test no. 4: $I_c = 20$ A, $\alpha = 0.15$, $I_d = 100$ A

$\int_{\tau_i}^{\tau_f} EI\,d\tau\|_{\text{charge}} + \int_{\tau_i}^{\tau_f} EI\,d\tau\|_{\text{overcharge}}$	3.02E + 06 J
$\int_{\tau_i}^{\tau_f} EI\,d\tau\|_{\text{charge}}$	84.93%
$\int_{\tau_i}^{\tau_f} EI\,d\tau\|_{\text{overcharge}}$	15.07%
$\int_{\tau_i}^{\tau_f} EI\,d\tau\|_{\text{discharge}}$	−71.52%
$C_{\text{bat}}(T_{\text{bat,f}} - T_{\text{bat,i}})$	−0.02%
$\sum$ losses	−28.33%
Residue	0.17%
$E(\tau_i)$	6.00 V
$E(\tau_f)$	6.03 V
$\Delta\tau$	118575 s

Table 4
Thermal balance by phase for test no. 3: $I_c = 20$ A, $\alpha = 0.15$, $I_d = 100$ A

Thermal balance by phase (W)	Charge	Overcharge	Rest	Discharge	Rest
EI	140.53	41.88	−0.18	−343.17	−0.03
$\dot{M}_{w,bat}c_w(T_{w,su,bat} - T_{w,ex,bat})$	1.19	−6.11	−5.29	−31.88	−5.86
$\sum A_{bat-j}(T_{amb} - T_{s,j})$	0.80	0.40	0.32	−1.02	0.30
$\dot{M}_{H_2}HHV_{H_2}$	0.28	15.99	0.00	0.00	0.00
$C_{bat}(\Delta t_{bat}/\Delta\tau)$	−0.59	10.11	−2.97	43.39	−5.41
$E_{th}I$	142.83	10.07	−2.18	−419.47	−0.18
τ (s)	18240	10860.00	30983	6290	52202

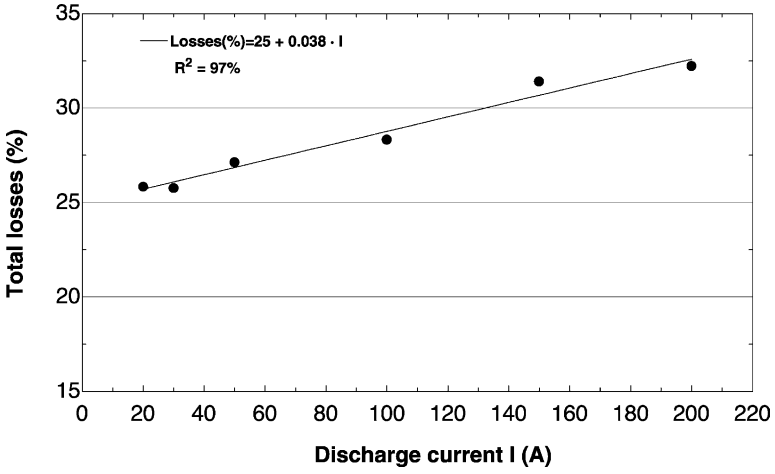

Fig. 8. Total losses vs. discharge current.

and discharging phases. Finally, Fig. 8 presents the influence of the discharge currents on the total losses. They vary from 26 to 32% for currents from 20 to 200 A. The varying losses in this case are mainly thermal losses to the cooling system and battery dynamic losses. The other types of losses remain almost constant.

7.2. Battery internal temperature

Fig. 9 shows the evolution of cell mean temperature during discharge, for different discharge rates and until the beginning of residual discharge. Mean temperature is defined as the temperature of the heart of the battery, calculated with the values given by thermocouples T_{c3} to T_{c7}, as shown in Fig. 4. It can be seen that increase in temperature is more important for higher discharge rates, partially due to higher Joule losses. Comparing the 20 and 200 A discharge rates, there is a difference of 25 K in the peak temperature reached.

7.3. Effect of discharge rate on thermoneutral voltage

Thermoneutral voltage is represented as a function of depth of discharge (DOD), for different discharge rates

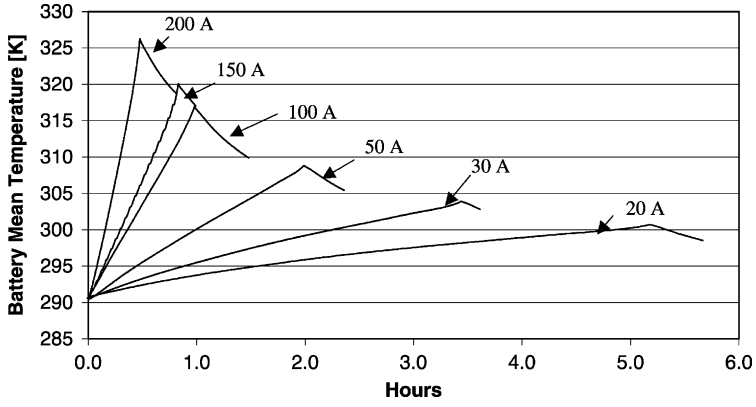

Fig. 9. Battery temperature evolution at different discharge rates.

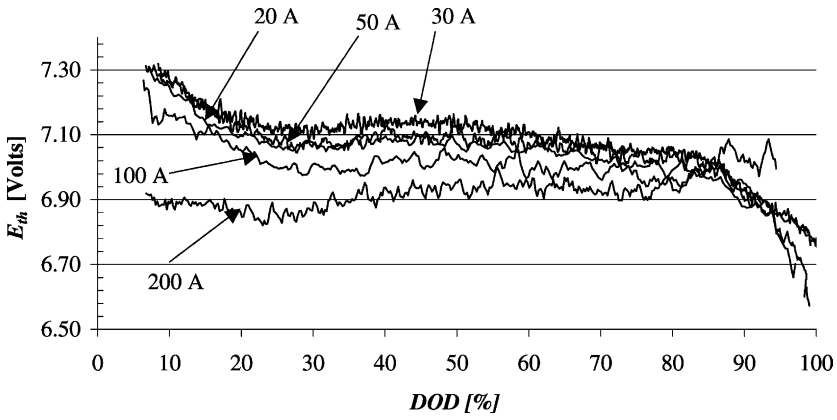

Fig. 10. E_{th} evolution during discharge.

(Fig. 10). DOD is defined by:

$$\mathrm{DOD}(\tau) = \left| \frac{\int_{\tau_i}^{\tau} I_d \, d\tau}{\mathrm{CAP}_{ref}} \right| \quad (26)$$

where CAP_{ref} is equal to 100 Ah. It can be observed that thermoneutral voltages for the 20, 30 and 50 A discharge rates are very close to each other. The 100 A thermoneutral voltage curve is slightly beneath the 20 and 30 A curves. The 200 A curve is totally different from the others: it is rising while DOD is raised. Curves for 20, 30 and 50 A discharge rates are near to the theoretical value which is five times 1.43 V (five cells in series), so it is 7.15 V. The theoretical thermoneutral voltage can be found according to the definition of E_{th} in Eq. (9), knowing the enthalpy variation of reaction (3).

7.4. Heat of reaction and entropy variation during discharge

With the discharge tests results, we could determine thermoneutral voltage E_{th} for a certain DOD and current intensity. Knowing the cell voltage, it is thus possible to calculate the first member of Eq. (19). If we plot the values of $(E_{th} - E)$, for a given DOD, as a function of discharge current intensity, we obtain a straight line, which can be seen on Fig. 11. It has to be noted that the coefficients of determination of this line are very close to unity. In order to know internal resistance, we calculate the slope of the line, which is equal to R. In order to determine cell entropy variation during discharge, we take the value of $(E_{th} - E)$ at the intersection of the Y-axis of the plot. We obtain:

$$(E - E_{th})_{I=0} = T \frac{\partial E_{eq}}{\partial T}$$

If we divide this quantity by T and multiply it by $z\,F$, we obtain the entropy variation during discharge, as shown in Eq. (10). All prior equations are valid only for isothermal process, which is obviously not the case for our cell discharges. So we decided to calculate on the mean cell temperature for the discharges at 20 and 30 A rates because these rates produce the least increase in cell temperature. The entropy variation calculated is expressed in ($\mathrm{J\,K^{-1}}$) and is relative to the whole battery. In order to give values in ($\mathrm{J\,K^{-1}\,mol^{-1}}$), we divide by five (five cells connected in series) and by two

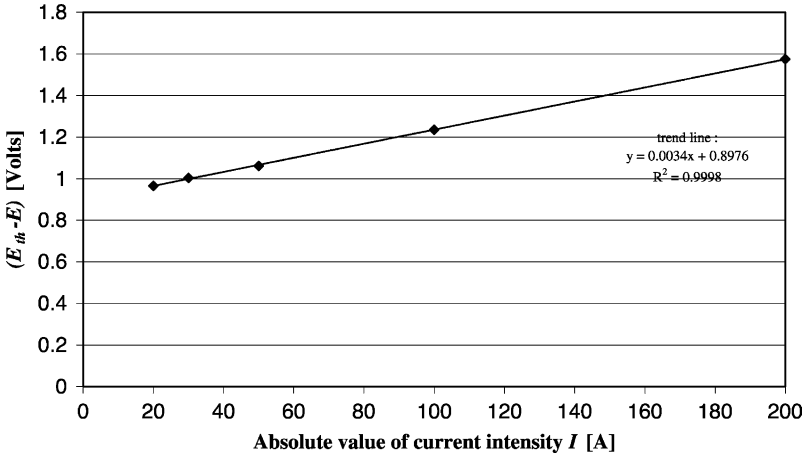

Fig. 11. The $(E_{th} - E)$ for DOD of 70%.

Table 5
Entropy variation of one cell, for 1 mol of electrons

	DOD								
	10%	20%	30%	40%	50%	60%	70%	80%	90%
$\Delta S\,(\mathrm{J\,K^{-1}\,mol^{-1}}) = F(\Delta E_{eq}/\Delta T)$	−50.7	−50.8	−52.3	−55.4	−56.8	−56.4	−57.9	−61.1	−57.4

Table 6
Heat produced due to entropic effect, during a discharge, for one cell and 1 mol of electrons

	DOD							
	10%	20%	30%	40%	50%	60%	70%	80%
$\dot{Q}_s\,(\mathrm{kJ\,mol^{-1}}) = FT(\Delta E_{eq}/\Delta T)$	−7.4	−7.5	−7.7	−8.2	−8.4	−8.4	−8.7	−9.2

because there are 2 mol of electrons transiting the cell during reaction. Entropy variation is given in Table 5.

The fact that entropy variation is negative during discharge fits well to common meaning of disorder associated to entropy: during discharge, 5 mol of reactants give only 3 mol of products and moreover, products are in an oxidized state, more stable that the reactant state. Heat generation due to entropic effect can also be obtained, recalling Eq. (14).

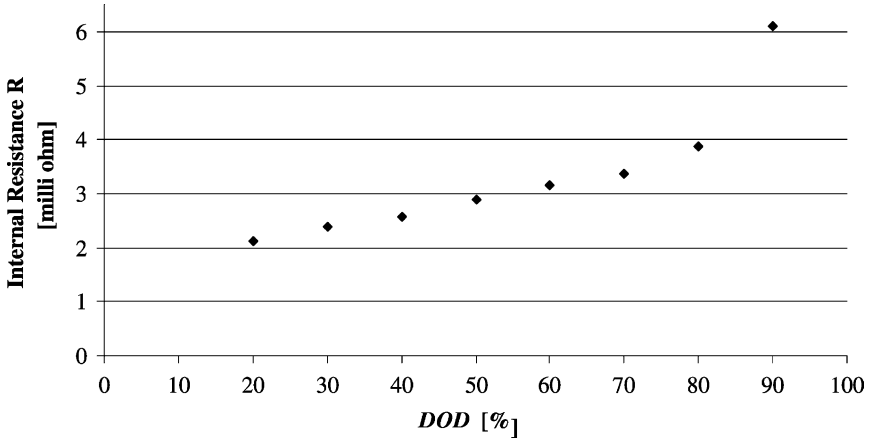

Fig. 12. Internal resistance R evolution during discharge.

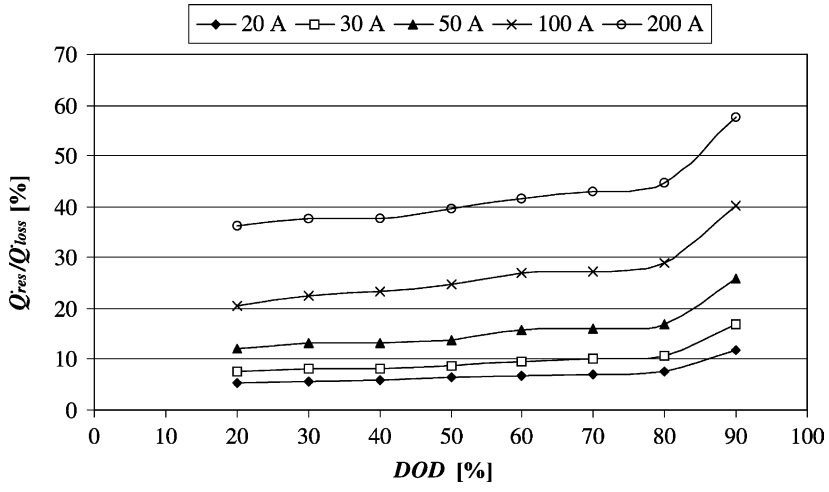

Fig. 13. Percentage of internal resistance heat generation in total heating power, during discharge.

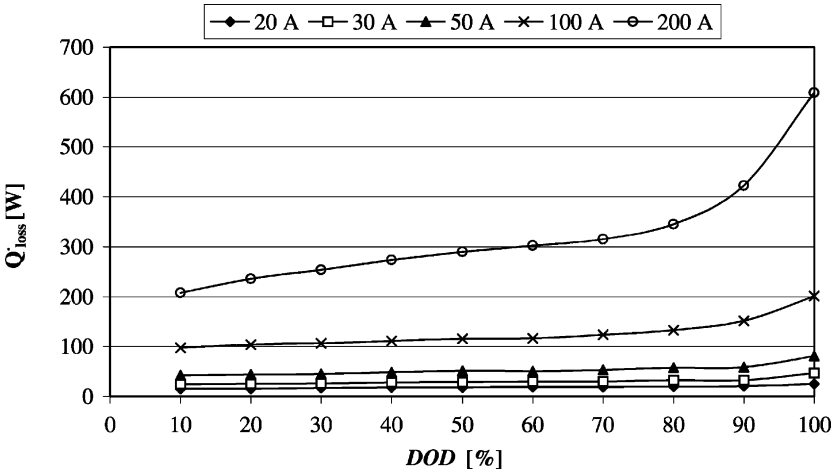

Fig. 14. Evolution of heating power during discharge.

In this case, the problem of definition of T disappears. Values are tabulated in Table 6, for one cell and 1 mol of electrons.

7.5. Determination of the internal resistance by thermal balance

Fig. 12 shows the evolution of internal resistance R (electric + polarization) in function of DOD calculated as explained herebefore. It can be seen that internal resistance is growing with the DOD.

7.6. Influence of the internal resistance on heating power

We have determined the internal resistance as a function of DOD, so that the power produced due to internal resistance can be calculated by Eq. (17). In Fig. 13, we represented the fraction of total heating power due to internal resistance, as a function of DOD and for various discharge rates. It can be observed that the percentage of internal resistance power in total heating power is growing when DOD is increasing, due to the fact that internal resistance is rising too. Obviously, the effect of internal resistance is more important for higher discharge currents. For the 20 A discharge, internal resistance heat generation compared to total heating power is about 6%, whereas for the 200 A discharge current, it reaches values of about 40%, for a DOD equal to 50%. As conclusion, it can be said that entropic effect has a greater influence on heat generation than internal resistance.

7.7. Total heating power evolution during a discharge

In Fig. 14, the evolution of total heating power as a function of DOD for different discharge rates is represented. While total heat generation in battery is relatively low for 20, 30 and 50 A discharge rates, total heating power is quite high for 100 and 200 A discharge rates, which generate a high increase of internal temperature of the battery.

8. Conclusions

In this paper, it was shown how an accurate calorimetric study can be used to analyze the different battery losses during typical charge–overcharge–rest–discharge cycles. It was shown that total losses range typically around 30% varying from 25 to 33% as the discharge current varies from 20 to 200 A. The different contributions of various losses during battery cycling are calculated. Mainly, the heat losses are found in the water cooling system during charge and discharge and in production of H_2 during overcharge. The temperatures measured in the cell block were analyzed at different discharge currents. Temperature increases up to 50 K were obtained for the highest discharge current, i.e. at 200 A.

Further, it was shown that it is possible to do more with such a heat balance: from extrapolation of the voltage curve obtained at different current intensities to zero intensity, it was possible to deduce entropy generation and also joule + polarization resistance at different DOD. An increase of the internal resistance from 2 to 6 mΩ was observed as the depth of discharge increased from 0 to 100%.

Acknowledgements

The authors wish to thank PSA-Citroën for their financial contribution to this project. Also Jules Hannay is gratefully thanked for his contribution to the experimental part of this study.

References

[1] P. Montalenti, P. Stangerup, Thermal simulation of Ni–Cd batteries for spacecraft, J. Power Sources 2 (1977–1978) 147–162.
[2] S. Al Hallaj, H. Maleki, J.S. Hong, J.R. Selman, Thermal modeling and design considerations of lithium batteries, J. Power Sources 83 (1999) 1–8.
[3] S. Al Hallaj, J. Prakash, J.R. Selman, Characterization of commercial Li-ion batteries using electrochemical-calorimetric measurements, J. Power Sources 87 (2000) 186–194.

[4] N. Sato, Thermal behavior analysis of lithium-ion batteries for electric and hybrid vehicles, J. Power Sources 99 (2001) 70–77.
[5] Y. Morioka, S. Narukawa, T. Itou, State-of-the-art of alkaline rechargeable batteries, J. Power Sources 100 (2001) 107–116.
[6] A.K. Shukla, S. Venugopalan, B. Hariprakash, Nickel-based rechargeable batteries, J. Power Sources 100 (2001) 125–148.
[7] L. David, Handbook of Batteries and Fuel Cells, McGraw-Hill, New York, 1984.
[8] F. Joubert, J. Bouet, J.-F. Fauvarque, Microcalorimetric studies of commercial Ni–Cd and Ni–Mh cells, in: C.F. Holmes, A.R. Landgrebe (Eds.), Proceedings of the Electrochemical Society on Batteries for Portable Applications and Electric Vehicles, vol. 97-18, PV 97-18, Paris, France, September 1997, ISBN 1-56677-146-3.